Top-down design of magnonic crystals from bottom-up magnetic nanoparticles through protein arrays

2017 Nanotechnology 28 155301

(http://iopscience.iop.org/0957-4484/28/15/155301)

IOP Publishing

Nanotechnology

Nanotechnology **28** (2017) 155301 (6pp)

https://doi.org/10.1088/1361-6528/aa62f3

Top-down design of magnonic crystals from bottom-up magnetic nanoparticles through protein arrays

M Okuda[1,2,3], T Schwarze[4], J-C Eloi[1,9], S E Ward Jones[1], P J Heard[5], A Sarua[1], E Ahmad[6,7], V V Kruglyak[6], D Grundler[4,8] and W Schwarzacher[1]

[1] University of Bristol, H. H. Wills Physics Laboratory, School of Physics, Tyndall Avenue, Bristol BS8 1TL, United Kingdom
[2] CIC nanoGUNE consolider, Avenida Tolosa 76, E-20018, Donostita-San Sebastian, Spain
[3] Ikerbasque, Basque Foundation for Science, María Díaz de Haro 3, 6ª planta, E-48013 Bilbao, Spain
[4] Technische Universität München, Physik Department, James-Franck-Str. 1, D-85747 Garching b. München, Germany
[5] University of Bristol, Interface Analysis Centre, Tyndall Avenue, Bristol BS8 1TL, United Kingdom
[6] University of Exeter, School of Physics, Stocker Road, Exeter EX4 4QL, United Kingdom
[7] The University of Manchester, School of Electrical and Electronic Engineering, Sackville Street, Manchester M13 9PL, United Kingdom
[8] Laboratory of Nanoscale Magnetic Materials and Magnonics (LMGN), Institute of Materials (IMX), Ecole Polytechnique Fédérale de Lausanne (EPFL), 1015 Lausanne, Switzerland

E-mail: okuda.mitsuhiro@selforganization.pro

Received 11 January 2017, revised 17 February 2017
Accepted for publication 24 February 2017
Published 15 March 2017

Abstract

We show that chemical fixation enables top-down micro-machining of large periodic 3D arrays of protein-encapsulated magnetic nanoparticles (NPs) without loss of order. We machined 3D micro-cubes containing a superlattice of NPs by means of focused ion beam etching, integrated an individual micro-cube to a thin-film coplanar waveguide and measured the resonant microwave response. Our work represents a major step towards well-defined magnonic metamaterials created from the self-assembly of magnetic nanoparticles.

Supplementary material for this article is available online

Keywords: self-assembly, magnetic nanoparticle, ferritin, chemical fixation, ferromagnetic resonance, magnonic metamaterial, magnonics

(Some figures may appear in colour only in the online journal)

1. Introduction

Inorganic nanoparticles (NPs) coated with surfactants can self-assemble via hydrophilic or hydrophobic interactions to form regular 2D or 3D structures (colloidal crystals) [1–8] and NPs coated with biological molecules, DNA or proteins can also form highly ordered structures with tunable lattice parameters [9, 10]. Many potential applications for such materials require their patterning into well-defined shapes and the exact positioning of the self-assembled superlattices. For example, thin sections of semiconductor colloidal crystals would be useful for electronic devices exploiting the charge storage capacity of the NPs [11] and shaped arrays of metal NPs for plasmonic devices [12].

To develop integrated devices containing functional NPs periodically arranged in three-dimensions, it is necessary to fabricate samples of the self-assembled 3D NPs arrays with well-defined geometries, often with flat surfaces, to precisely

[9] Present address: Wolfson Center, Institute of Material and Manufacturing, Brunel University London, Kingston Lane, Uxbridge UB8 3PH, United Kingdom.

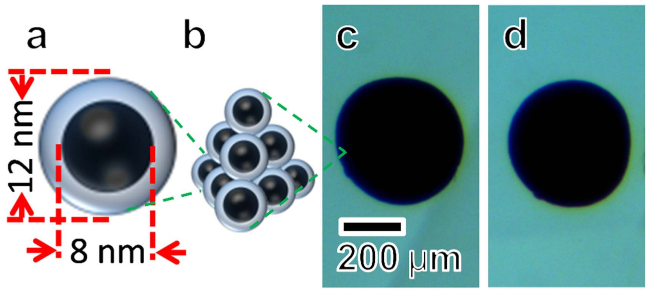

Figure 1. Schematic and images of Fe_3O_4–ferritin crystals. (a) Schematic of monomer of Fe_3O_4–ferritin. (b) Schematic of crystals of Fe_3O_4–ferritin and optical images of crystals of Fe_3O_4–ferritin before (c) and after chemical fixation (d). Green broken lines show the scale relationship between the schematics and the image.

generate and analyze electric and magnetic properties. This is in particular true for superlattices consisting of ordered magnetic particles. Here, the long-range magnetic stray fields and demagnetization effect depend critically on the surfaces and alter the internal magnetic field. The internal magnetic field rules the microwave response and spin-wave (magnon) modes [13] which are of relevance in very different fields ranging from biomedicine [14] to microwave devices [15] and magnonics [16]. Non-flat or irregular surfaces do not allow one to precisely determine the demagnetization factors necessary for a detailed data analysis. At the same time three-dimensionally arranged nanoparticles are expected to exhibit lattice-induced anisotropic properties that might be compromised by irregular shapes. Therefore, a method to machine an exact shape and size with well-defined surfaces is indispensable for device development and applications while still keeping the periodicity of the NPs. Also precise positioning of the machined structure is of utmost importance.

Thin sections of magnetic NPs are of special interest for their magnetotransport properties [17] and for use in magnetic devices operated at microwave frequencies [14–16]. Often, randomly oriented magnetic NPs have been addressed [14, 15, 18]. In the research field of magnonics, however, strictly periodic magnetic nanostructures that form artificial crystals are of crucial interest [16]. To fully exploit the rich advantages offered by magnonics technology, it was very recently argued that mastering spin waves with sub-100 nm wavelengths is key [19].

Here, artificial crystals with feature sizes on the 10 nm length scales are a prerequisite to efficiently control and manipulate such waves. Top-down state-of-the-art nanolithography does not allow for such tiny pitches. Inverse opal structures fabricated from magnetic materials using a bottom-up approach exhibited periods that ranged from 366 to 800 nm [20–22] and were thus far too large. Appropriate micro-machining has not yet been reported either as most self-organized structures are very fragile with only weak electrostatic interactions between the NPs. Additional covalent bonds are required to maintain the internal structure stable against the external stress caused by machining a well-defined outer shape.

We report here a bottom-up grown and micromachined magnetic superstructure that is periodically patterned in all three spatial directions. The lattice constant is 12 nm. The protein-coated magnetic NPs that we used have a particular advantage because of the amino acids on the protein surface that generate additional covalent bonds stabilizing the spatial arrangement. At the same time, protein-coated NPs are easily assembled into very large periodic 3D arrays by crystallization [9]. Importantly, we found that after cross-linking the protein crystals with glutaraldehyde, the self-assembled NP arrays retained their periodic structure after micro-machining into a micro-cube via focused-ion-beam (FIB) milling. Although there have been previous reports using glutaraldehyde to fix nanostructures [23], the application to top-down patterning of periodic NP arrays is new. This allowed us to integrate the micro-cube into a coplanar wave guide and detect the magnetic resonance of the NPs at microwave frequencies. The observation magnetic NPs keep their functionality, so that precisely defined 3D magnonic metamaterials for on-chip integration now become feasible.

2. Experiments

2.1. Synthesis, purification and crystallization of Fe_3O_4–ferritin

The synthesis process followed a modified procedure from the literature [24] and all the processes were reported previously [9]. Dried Fe_3O_4–ferritin crystals were fixed by immersion in 2.5% glutaraldehyde, 40 mM cadmium sulfate and 50 mM Tris-HCl (buffer: pH 8.0) for 48 h. Hydrated apoferritin crystals were fixed by immersion in 2.5% glutaraldehyde, 40 mM cadmium sulfate and 50 mM HEPES-NaOH (buffer: pH 8.0) for 48 h.

2.2. Measurement of microwave absorbance

The insulating cubic crystal was fixed on a coplanar waveguide (CPW) prepared on a semi-insulating GaAs substrate. A magnetic field $\mu_0 H$ of 0.5 T was applied perpendicular to the substrate. Microwave probes connected the CPW to a vector network analyzer that provided a sinusoidal radio-frequency voltage signal with frequencies ranging from 10 MHz to 26.5 GHz [25]. The accompanying microwave magnetic field stimulated spin-precessional motion in the NPs leading to voltage induction in the metallic signal line of the CPW. The absorption spectra were extracted from scattering parameters measured on the CPW. To enhance the signal-to-noise ratio and determine the H-dependent dynamic response a reference spectrum taken at $\mu_0 H = 1$ T was subtracted from the datasets. As both a varying temperature and a large H modified the baselines of the reference spectra, the off-resonance signal levels as shown in figure 4 are different.

3. Results and discussion

We use magnetite NPs templated by the iron storage protein apoferritin (Fe_3O_4–ferritin) [9]. Apoferritin consists of an empty protein shell of outer diameter 12 nm and inner diameter 8 nm (figure 1(a)) [26] and has been used as a template for a wide range of inorganic NPs [27–30]. The uniform Fe_3O_4-NPs are synthesized within the central protein cavity and assembled into periodic 3D face-centered cubic arrays of synthetic magnetic NPs through a method previously reported by our group [9]. Our NP arrays are similar to colloidal crystals, except that each NP is located in the central cavity of an apoferritin molecule, and they are formed by specific protein–protein interactions mediated by cadmium ions [9, 27] rather than isotropic interactions between surfactant-coated NPs. Other cage-shaped proteins and viruses can also form spherical NPs in their central cavities [31–35] while tube-like viruses can form nanorods [36]. There are therefore numerous possible alternatives to apoferritin as a basis for micro-machined periodic NP arrays.

Although periodic NP arrays with dimensions up to several hundred μm or larger can be fabricated by this method [9], it remains difficult to control their overall size and shape, so that an appropriate patterning method is required in order to form arbitrarily shaped structures. The FIB has proven an exceptionally versatile tool for shaping inorganic materials such as semiconductors and metals [37] but an additional strengthening step is required before it can be applied to fragile, self-assembled arrays. We therefore apply chemical fixation to the protein-NP crystals and show that this permits their machining using dual-beam FIB/scanning electron microscopy (SEM). Crystals of Fe_3O_4–ferritin were chemically fixed using glutaraldehyde as a crosslinker, and cut to shape by FIB.

Glutaraldehyde crosslinks proteins through the alkylation of lysine residues and other α-amino groups [38, 39], and is employed for instance when microtoming biological structures. Figures 1(c) and (d) show crystals of Fe_3O_4–ferritin before and after chemical fixation by a glutaraldehyde solution (2.5% glutaraldehyde, 40 mM cadmium sulfate and 50 mM Tris-HCl buffer, pH 8.0). Cadmium sulfate and Tris-HCl buffer were used in the fixation solution as well to reduce the possibility of Fe_3O_4–ferritin crystal destruction due to buffer displacement in the crystal.

Crystals of Fe_3O_4–ferritin with and without chemical fixation were allowed to dry, and then fixed to the FIB sample-holder using conductive silver paste. An earlier small angle x-ray diffraction study showed that the lattice parameter of the Fe_3O_4–ferritin crystal reduces from 18.5 to 15.5 nm on drying [9]. The crystals were coated with several nanometers thick Pt within the FIB/SEM instrument to allow initial imaging (SEM) and machining (FIB) (see online supplementary figure S1, available at stacks.iop.org/NANO/28/155301/mmedia). Figure 2(a) shows a rectangular hole fabricated by the FIB at the center of a crystal fixed with glutaraldehyde. Figure 2(b) is a magnified image of the inner surface of the hole, and shows that the magnetic NPs remain discrete. They do not fuse with each other and, crucially, still

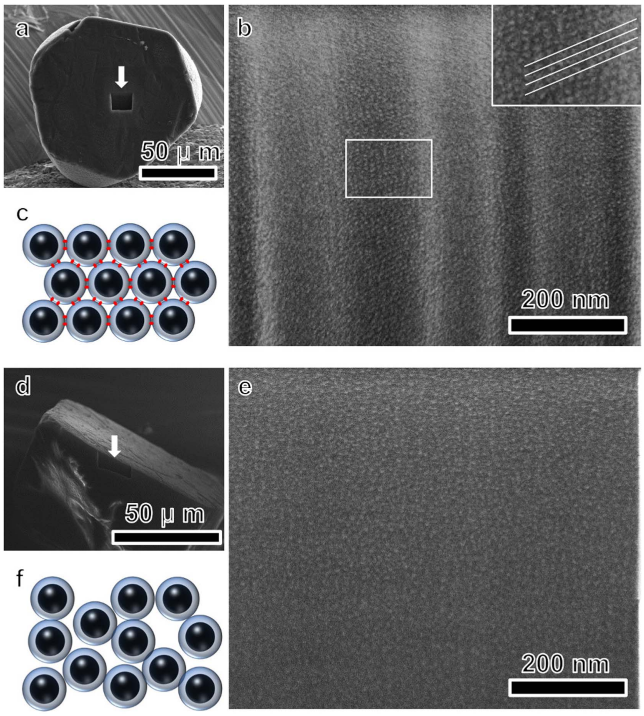

Figure 2. SEM images of Fe_3O_4–ferritin crystals cut by FIB. (a) SEM image of the surface of a Fe_3O_4–ferritin crystal fixed by glutaraldehyde. The rectangular hole at the center is the area machined by the FIB (white arrow). (b) High magnification SEM image of the cut area in (a). The NPs appear as a regular array of white dots. (Inset in (b)) Magnified image of the region outlined by the white rectangle in (b). The white lines are guides to the eye, approximately parallel to the lines of white dots visible in the image. The aligned white dots between lines are NPs, and their alignment means that NPs on the surface of the crystal are ordered. (c) A schematic of aligned ferritin observed in (b). Red parts indicate glutaraldehyde crosslinking ferritins. (d) SEM image of the surface of a Fe_3O_4–ferritin crystal without fixation by glutaraldehyde. The area machined by the FIB is indicated by a white arrow. (e) High magnification SEM image of the cut area shown in (d). Here, the NPs (white dots) are no longer ordered. (f) A schematic of randomly orientated ferritin illustrating (e).

form a periodic array. The periodic structure is seen to be continuous across almost the whole surface area.

Without fixation, the cut surface of a protein–NP crystal no longer maintains its periodicity. Figure 2(d) shows a rectangular hole machined by FIB at the edge of a Fe_3O_4–ferritin crystal without fixation. Figure 2(e) is a magnified image of the inner surface of the hole, and shows that the NPs no longer form a periodic array. Our results indicate that chemical fixation with glutaraldehyde is indispensable when cutting protein crystals using FIB. Glutaraldehyde promotes a crosslinking with proteins through alkylation of lysine residues and other α-amino groups. Therefore, the covalent bonds between proteins can maintain the periodic structure against the Ga ion beam (figure 2(c)). The structure without the covalent bonds is fragile against a Ga ion beam and shows randomly orientated NPs after the machining (figure 2(f)).

With this in mind, thin sections of Fe_3O_4–ferritin crystals with crosslinking were fabricated (figure 3(a)) using a FIB cutting procedure to confirm the presence of ordered NPs

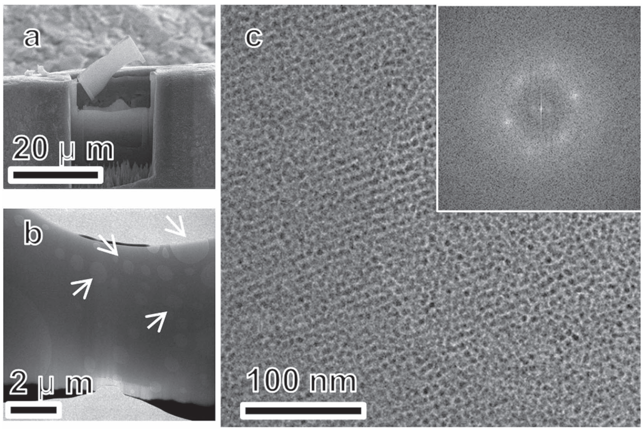

Figure 3. SEM and TEM images of a thin section of Fe_3O_4–ferritin crystal fabricated by FIB. (a) SEM image of a thin section of a Fe_3O_4–ferritin crystal fabricated by FIB. (b) Low magnification TEM image of the thin section from (a) on a TEM grid. White arrows show the holes of the holey carbon TEM grid. (c) High magnification TEM image of the upper central area of the thin section in (b) with FFT (inset).

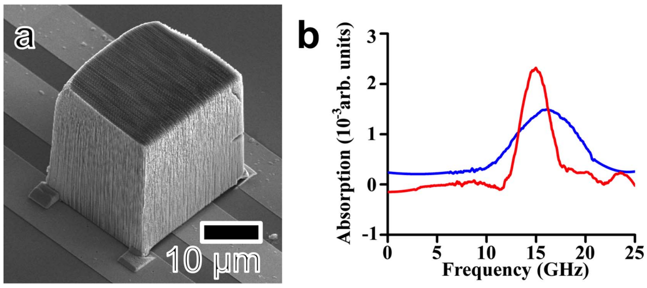

Figure 4. A SEM image and microwave absorption spectra of a cubic Fe_3O_4–ferritin crystal fabricated by FIB. (a) SEM image of a cube cut from an insulating Fe_3O_4–ferritin crystal fixed to the two outer ground lines of a coplanar waveguide (light-gray leads). (b) Microwave absorption spectra taken in an external magnetic field of 0.5 T applied in a direction perpendicular to the substrate (red line: 290 K, blue line: 5 K).

despite the influence of the Ga ion beam (see supporting information figure S2). As illustrated in figure 3, a thin section of the crystal could be placed on a holey carbon grid for transmission electron microscopy (TEM) imaging and the central area was sufficiently thin to create a good TEM image contrast. The round shapes (white arrows) in the low-magnification TEM image (figure 3(b)) are holes of the holey carbon membrane. High magnification TEM images show the periodic structure (figure 3(c)) of the magnetic NPs. Each particle is discrete and does not fuse with its neighbors, indicating that the Ga ion beam does not affect the arrangement of the protein-coated NPs in a thin section. These results highlight the role of glutaraldehyde as a crosslinker, maintaining the integrity of the crystal's periodicity. A fast Fourier transformation (FFT) shows six clear spots (inset of figure 3(c)), evidencing that the periodicity of the superstructure was maintained when cutting with a Ga ion beam. The periodicity was observed over the whole central area of the section (approximately $6\,\mu m \times 4\,\mu m$ in size), which places a lower limit on the size of any grains in the crystal. Outside this area the thickness was too large for TEM contrast. Further thinning was not possible due to bending of the 20 nm thick sections cut by FIB, it is because the stiffness of the 20 nm thin section was not large enough to retain them without support. It is reasonable to assume that Ga ion implantation took place into the top surface of the cut area. For Ga ions at 30 keV, the implantation depth is 50 nm [40]. Still, the periodicity was clearly maintained even in the thin sections.

As a further demonstration of micromachining of self-organized NP assemblies with crosslinking, we created a 3D structure, namely a $50\,\mu m \times 50\,\mu m \times 40\,\mu m$ microcube out of a periodic NP array. The outer dimensions of the microcube were optimized to bridge the separation between two ground lines of a CPW as shown in figure 4(a). The SEM images indicated a stripe-like surface roughness of the side walls occurring parallel to the Ga ion beam. Its root-mean-square value amounted to about 60 nm. We assume that the stripe-like roughness can be reduced by optimizing the intensity and spot size of the Ga ion beam. Fixed with Pt at its corners, the insulating microcube was centered on top of the signal line of the CPW. The configuration allowed us to perform broadband spin-wave spectroscopy by applying a microwave current to the signal line. The current generated a radio frequency (rf) magnetic field that exerted a torque on the spins of the magnetic NPs. Figure 4(b) shows the microwave absorption measured in an applied field of 0.5 T as a function of frequency for two different temperatures. The magnetic resonance peak observed around 15 GHz was sharper at 290 K compared to 5 K which is below the blocking temperature of the magnetic NPs [9]. Considering the small implantation depth of 50 nm compared to the microcube's side length of 40–50 μm, only a small amount of Fe_3O_4 NPs were possibly modified and disordered through Ga ions. This amount does not explain the relatively large linewidth of the resonance peak. For the experiments at 5 K, the Fe_3O_4–ferritin crystal is below its blocking temperature and the ferromagnetic resonance linewidth is expected to be broadened as the crystal lattices of individual nanoparticles are misaligned with respect to each other. The inhomogeneous broadening can be estimated from the anisotropy [41]. Assuming an anisotropy field derived from the blocking temperature of 18 K, we estimate a linewidth of 6.8 GHz that agrees reasonably well with the experimentally observed full width at half maximum in figure 4(b) [42]. From these results, we attribute the low temperature broadening to the influence of the magnetic anisotropy of the NPs. However, further work will be required to confirm this phenomenon. A detailed analysis of lineshapes and resonance frequencies will be given elsewhere. Theoretical work suggests that ordered NP assemblies hold considerable promise as magnonic metamaterials [43]. Our results now pave the way for shape-tailored NP arrays that are optimized for integration in microwave antennas. The approach to a magnonic meta-material presented here is complementary to inverse opal structures [21, 22]. The insulating protein-matrix is expected to reduce eddy current losses compared to a conductive bulk material utilized in microwave applications.

4. Conclusion

Chemically fixed protein/inorganic-NP composite crystals were prepared and machined into stable artificial structures at room temperature by combining crosslinking and FIB techniques. The chemical fixation retained the periodic NPs structure without loss of order by FIB. The precision of the FIB beam position is $\sim$5 nm and it is hence possible to machine sections as thin as 20 nm by this method. Our methods open a route to fabricating periodic 3D NP arrays of tailored shape. In addition, using magnetic Fe_3O_4–ferritin crystals we showed the ferromagnetic resonance in FIB-processed periodic 3D NP arrays, for the first time. With a modified cross-linking step, the methods presented here could be applied to colloidal crystals formed from arrays of chemically functionalized NPs as well as protein-templated NP arrays for a wide variety of applications [44, 45].

Acknowledgments

The research leading to these results has received funding from the European Community's Seventh Framework Programme (FP7/2007–2013) under Grant Agreement n°228673 (MAGNONICS). This work was carried out with the support of the Bristol Centre for Nanoscience and Quantum Information and the Cluster of Excellence 'Nanosystems Initiative Munich'. TS and DG thank M Krawczyk for discussions.

References

[1] Shevchenko E V, Talapin D V, Kotov N A, O'Brien S and Murray C B 2006 *Nature* **439** 55
[2] Talapin D V, Shevchenko E V, Bodnarchuk M I, Ye X, Chen J and Murray C B 2009 *Nature* **461** 964
[3] Choi J J, Bealing C R, Bian K, Hughes K J, Zhang W, Smilgies D-M, Hennig R G, Engstrom J R and Hanrath T 2011 *J. Am. Chem. Soc.* **133** 3131
[4] Nykypanchuk D, Maye M M, van der Lelie D and Gang O 2008 *Nature* **451** 549
[5] Park S Y, Lytton-Jean A K R, Lee B, Weigand S, Schatz G C and Mirkin C A 2008 *Nature* **451** 553
[6] Jones M R, Macfarlane R J, Lee B, Zhang J, Young K L, Senesi A J and Mirkin C A 2010 *Nat. Mater.* **9** 913
[7] Sun S H, Murray C B, Weller D, Folks L and Moser A 2000 *Science* **287** 1989
[8] Yan J, Chen Z, Jiang J, Tan L and Zeng X C 2009 *Adv. Mater.* **21** 314
[9] Okuda M, Eloi J-C, Ward Jones S E, Sarua A, Richardson R and Schwarzacher W 2012 *Nanotechnology* **23** 415601
[10] Maye M M, Kumara M T, Nykypanchuk D, Sherman W B and Gang O 2010 *Nat. Nanotechnol.* **5** 116
[11] Yamada K, Yoshii S, Kumagai S, Fujiwara I, Nishio K, Okuda M, Matsukapaswa N and Yamashita I 2006 *Japan J. Appl. Phys.* **45** 4259
[12] Anker J N, Hall W P, Lyandres O, Shah N C, Zhao J and Van Duyne R P 2008 *Nat. Mater.* **7** 442
[13] Gurevich A G and Melkov G A 1996 *Magnetization Oscillations and Waves* (Boca Raton, FL: CRC Press)
[14] Yao B M, Gui Y S, Worden M, Hegmann T, Xing M, Chen X S, Lu W, Wroczynskyj Y, van Lierop J and Hu C-M 2015 *Appl. Phys. Lett.* **106** 142406
[15] Song N N, Yang H T, Liu H L, Ren X, Ding H F, Zhang X Q and Cheng Z H 2013 *Sci. Rep.* **3** 3161
[16] Kruglyak V V *et al* 2012 Magnonic metamaterials *Metamaterial* (Rijeka, Croatia: InTech) pp 341 www.intechopen.com/books/metamaterial/magnonic-metamaterials
[17] Zeng H, Black C T, Sandstrom R L, Rice P M, Murray C B and Sun S 2006 *Phys. Rev.* B **73** 020402(R)
[18] De Biasi E, Ramos C A and Zysler R D 2003 *J. Magn. Magn. Mater.* **262** 235
[19] Chumak A V, Vasyuchka V I, Serga A A and Hillebrands B 2015 *Nat. Phys.* **11** 453
[20] Kostylev M *et al* 2012 *Phys. Rev.* B **86** 184431
[21] Pascu O, Caicedo J M, López-García M, Canalejas V, Blanco A, López C, Arbiol J, Fontcuberta J, Roig A and Herranz G 2011 *Nanoscale* **3** 4811
[22] Abramova V V, Slesarev A and Sinitskii A 2013 *J. Mater. Chem.* C **1** 2975
[23] Harrison P M and Arosio P 1996 *Biochim. Biophys. Acta* **1275** 161
[24] Klem M T, Resnick D A, Gilmore K, Young M, Idzerda Y U and Douglas T 2007 *J. Am. Chem. Soc.* **129** 197
[25] Schwarze T and Grundler D 2013 *Appl. Phys. Lett.* **102** 222412
[26] Falkner J C, Turner M E, Bosworth J K, Trentler T J, Johnson J E, Lin T and Colin V L 2005 *J. Am. Chem. Soc.* **127** 5274
[27] Okuda M, Suzumoto Y and Yamashita I 2011 *Cryst. Growth Des.* **6** 2540
[28] Meldrum F, Heywood B and Mann S 1992 *Science* **257** 522
[29] Uchida M, Klem M T, Allen M, Suci P, Flenniken M, Gillitzer E, Varpness Z, Liepold L O, Young M and Douglas T 2007 *Adv. Mater.* **19** 1025
[30] Klem M T, Young M and Douglas T 2010 *J. Mater. Chem.* **20** 65
[31] Okuda M, Suzumoto Y, Iwahori K, Kang S, Uchida M, Douglas T and Yamashita I 2010 *Chem. Commun.* **46** 8797
[32] Kang S, Oltrogge L M, Broomell C C, Liepold L O, Prevelige P E, Young M and Douglas T 2008 *J. Am. Chem. Soc.* **130** 16527
[33] Resnick D A, Gilmore K, Idzerda Y U, Klern M T, Allen M, Douglas T and Arenholz E 2006 *J. Appl. Phys.* **99** 08Q501
[34] Douglas T and Young M 1998 *Nature* **393** 152
[35] de la Escosura A, Verwegen M, Sikkema F D, Comellas-Aragones M, Kirilyuk A, Rasing T, Nolte R J M and Cornelissen J J L M 2008 *Chem. Commun.* **13** 1542
[36] Knez M, Bittner A M, Boes F, Wege C, Jeske H, Maiß E and Kern K 2003 *Nano Lett.* **3** 1079
[37] Giannuzzi L A and Steivie F A 2005 *Introduction to Focused Ion Beams—Instrumentation, Theory, Techniques and Practice* (Berlin: Springer)
[38] Sung H W, Huang R N, Huang L L H, Tsai c.c.C C and Chiu C T 1998 *J. Biomed. Mater. Res.* **42** 560
[39] McIntosh D B 1992 *J. Biol. Chem.* **267** www.jbc.org/content/267/31/2232822328
[40] Thompson K, Gorman B P, Larson D J, van Leer B and Hong L 2006 *Microsc. Microanal.* **12** (suppl. 2) 1736–7
[41] Gurevich A G and Melkov G A 1996 *Magnetization Oscillations and Waves* (Boca Raton, FL: CRC Press)
[42] Schwarze T 2013 Spin waves in 2D and 3D magnonic crystals: from nanostructured ferromagnetic materials to chiral

helimagnets *PhD Thesis* Technische Universität München, Germany
[43] Mamica S, Krawczyk M, Sokolovskyy M L and Romero Vivas J 2012 *Phys. Rev.* B **86** 144402
[44] Zeth K, Hoiczyk E and Okuda M 2016 *Trends Biochem.* **41** 190
[45] Calò A, Eiben S, Okuda M and Bittner A M 2016 *Japan J. Appl. Phys.* **55** 03DA01